Research Papers

Green and Sustainable MEMBRANES

Green and Sustainable Membranes
Vol. 1, No. 1, June 2026
https://doi.org/10.62755/gsmb.2026.04

Check for updates

Effect of Natural Zeolite Loading in Electrospun PAN/PVP Nanofiber Membranes on the Adsorption of Cationic Dye (Methylene Blue)

Shalfa Fauza Alfidru[1], Istiara Rizqillah Hanifah[1], Rizky Aflaha[2], Aditya Rianjanu[1,*]

[1] *Department of Materials Engineering, Faculty of Industrial Technology, Institut Teknologi Sumatera, Terusan Ryacudu, Way Hui, Jati Agung, Lampung Selatan 35365, Indonesia*
[2] *Department of Physics, Faculty of Mathematics and Natural Sciences, Universitas Gadjah Mada, Sekip Utara PO Box BLS 21, Yogyakarta 55281, Indonesia*

Corresponding author: aditya.rianjanu@mt.itera.ac.id

ARTICLE HISTORY: Received: February 20, 2026 | Revised: March 30, 2026 | Accepted: April 20, 2026

ABSTRACT

Textile effluents containing cationic dyes such as methylene blue (MB) pose persistent environmental and health risks, and practical adsorbents must combine high capacity with ease of recovery. Here we report electrospun polyacrylonitrile/polyvinylpyrrolidone (PAN/PVP) nanofiber membranes loaded with natural zeolite (clinoptilolite, Tanggamus, Indonesia) at four levels (0, 0.1, 0.3, and 0.5 g; denoted PAN/PVP, PAN/PVP/Ze1, PAN/PVP/Ze3, and PAN/PVP/Ze5). The as-spun membranes were thermally stabilized at 200 °C under N_2 and characterized by SEM, EDS, XRD, and FTIR. Scanning electron microscopy revealed continuous, bead-free fibers whose mean diameter increased monotonically from 626±57 to 902±68 nm with zeolite loading, while EDS showed a simultaneous rise of Si (0 → 10.68 wt%) and Al (0.37 → 2.90 wt%). Progressive emergence of clinoptilolite reflections at $2\theta \approx 22.5^{\circ}$ and 29.6° in the XRD patterns and a red-shifting Si–O–Si/Si–O–Al asymmetric stretching band (1067 → 1040 cm^{-1}) in the FTIR spectra confirmed that the zeolite framework was preserved and its effective content increased with loading, without perturbing the PAN (~2242 cm^{-1} C≡N) or PVP (~1659 cm^{-1} C=O) signatures. In 10 ppm MB adsorption tests, PAN/PVP/Ze5 achieved ~100% dye removal after 300 min with an experimental adsorption capacity of 14.0 mg g^{-1}, compared with 58.7% and 8.2 mg g^{-1} for the pristine PAN/PVP control. The kinetic data for all samples were well described by the pseudo-second-order model ($R^2 \geq 0.984$), indicating a chemisorption-controlled uptake dominated by electrostatic and ion-exchange interactions with the aluminosilicate framework. The results demonstrate that natural-zeolite-loaded PAN/PVP nanofiber membranes are a low-cost, recoverable, and composition-tunable platform for cationic-dye wastewater treatment.

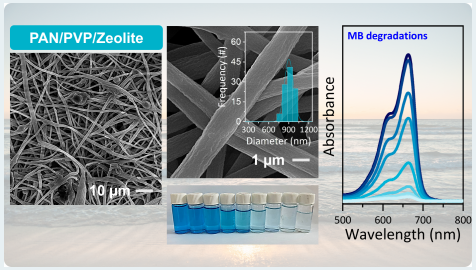

Keywords: *electrospinning; PAN/PVP nanofiber; natural zeolite; clinoptilolite; methylene blue; adsorption kinetics*

1. Introduction

Synthetic dyes discharged from textile, printing, leather, and paper industries constitute one of the largest sources of coloured wastewater worldwide, with hundreds of thousands of tonnes released annually into surface waters [1,2]. Methylene blue (MB), a thiazine cationic dye, is widely used as a model pollutant because of its intense absorption at 664 nm, slow biodegradation, and documented toxicity to aquatic organisms and humans at low concentration. Residual MB in effluents impairs photosynthesis by reducing light penetration, induces ocular and respiratory irritation upon exposure, and is difficult to remove by conventional primary treatment. The development of efficient, low-cost, and easily recoverable adsorbents for MB remains therefore a central goal of dye-wastewater research [3,4,5].

Among the available removal strategies (coagulation, membrane filtration, advanced oxidation, and adsorption) [6,7,8], adsorption is the most practical choice at small-to-medium scale because it is simple to operate, requires no complex reagents, and can achieve near-complete removal when the adsorbent is well matched to the dye chemistry [9,10]. Activated carbon, clays, biochar, and natural zeolites have all been investigated as bulk adsorbents, but powder-form adsorbents suffer from difficult recovery, secondary pollution, and pressure drop in column operation [11,12,13]. Immobilizing the active phase in a self-supporting membrane eliminates these drawbacks [14,15]. Electrospun polymer nanofibers are particularly attractive for this purpose: their interconnected porosity, high surface-to-volume ratio, mechanical integrity, and tunable chemistry make them a versatile host for functional fillers, and the resulting nanofibrous mat can be handled, regenerated, and reused as a single piece [16,17,18,19].

Polyacrylonitrile (PAN) is one of the most widely used electrospinning matrices for adsorbent membranes because its nitrile groups provide polar sites for interaction with cationic species and its backbone is chemically and thermally stable. Polyvinylpyrrolidone (PVP) is commonly blended with PAN to improve spinnability, increase hydrophilicity, and promote pore interconnection during post-treatment [20,21,22]. On the filler side, natural zeolite, in particular clinoptilolite, a microporous aluminosilicate characterized by channels populated with exchangeable Na^+, K^+, and Ca^{2+} cations, offers a large cation-exchange capacity toward

cationic dyes and is abundantly available as a low-cost mineral in several regions of Indonesia, including the Tanggamus area of Lampung Province [23,24,25]. Incorporating natural zeolite into PAN/PVP nanofibers should therefore combine the recoverability of a polymer membrane with the ion-exchange selectivity of the mineral, producing a hybrid adsorbent that is inexpensive, locally sourced, and easy to deploy.

Although several recent studies have examined PAN-based nanofiber adsorbents loaded with engineered metal oxides or synthetic zeolites [26,27], systematic work on natural-zeolite-loaded PAN/PVP nanofibers with a loading series spanning pristine to high filler content, full structural characterization, and quantitative kinetic analysis of MB adsorption is still scarce. In this work we address this gap by preparing electrospun PAN/PVP membranes with four zeolite loadings (0, 0.1, 0.3, and 0.5 g of Tanggamus clinoptilolite) under otherwise identical spinning conditions, thermally stabilizing them at 200 °C under N_2, and characterizing their morphology, composition, crystalline structure, and chemical bonding by SEM, EDS, XRD, and FTIR. The MB uptake kinetics at 10 ppm initial concentration are quantified over 300 min and fitted to pseudo-first-order and pseudo-second-order models to identify the rate-limiting step. The results reveal a monotonic enhancement of both adsorption rate and equilibrium capacity with zeolite loading, culminating in essentially complete MB removal at the highest loading, and establish natural zeolite from Tanggamus as an effective, low-cost functional filler for PAN/PVP adsorbent nanofibers.

2. Materials and Methods

2.1 Materials

Polyacrylonitrile (PAN, $M_w = 150,000$ g mol^{-1}) and polyvinylpyrrolidone (PVP, $M_w \approx 1,300,000$ g mol^{-1}) were obtained from Sigma-Aldrich (Singapore). *N*,*N*-Dimethylformamide (DMF, Merck, Germany) was used as the common solvent. Natural zeolite (clinoptilolite) was supplied by PT Paragon Perdana Mining and mined from Tanggamus, Lampung Province, Indonesia. The as-received zeolite was ground, sieved through a 200-mesh screen, and dried at 80 °C for 6 h before use. Methylene blue (MB, C.I. 52015, Merck, Germany) was selected as a representative cationic dye pollutant. Deionized water was used throughout. All chemicals were used as received.

2.2 Preparation of PAN/PVP/Zeolite nanofiber membranes

A base polymer solution was prepared by dissolving 0.8 g of PAN and 0.5 g of PVP in 10 mL of DMF at 60 °C under magnetic stirring (600 rpm, 4 h) until a transparent, viscous, and homogeneous dope was obtained. Four separate batches were then prepared by incorporating 0, 0.1, 0.3, and 0.5 g of sieved natural-zeolite powder into individual aliquots of the base solution, followed by an additional 2 h of stirring and 30 min of ultrasonication to promote uniform dispersion. The corresponding samples are designated **PAN/PVP**, **PAN/PVP/Ze1**, **PAN/PVP/Ze3**, and **PAN/PVP/Ze5**, where the numerical suffix indicates the zeolite mass in tenths of a gram (Table 1).

Electrospinning was carried out on a digital spinning platform (ILMI-N101, Integrated Laboratory of Materials and Instrumentation, Bandung, Indonesia). Each solution was loaded into a 10 mL plastic syringe fitted with a 21-gauge stainless-steel needle and deposited onto a rotating drum collector under the following fixed conditions: applied voltage 9 kV, feed rate 0.5 mL h^{-1}, needle-to-collector distance 10 cm, and collection time 16 h, at ambient temperature and humidity. The as-spun membranes were peeled from the collector and dried at 60 °C. All samples were subsequently subjected to a post-spin heat treatment at 200 °C for 2 h in a tube furnace under N_2 atmosphere at a heating rate of 5 °C min^{-1} to promote partial cyclization of the PAN backbone while preserving the zeolite framework and the overall fibrous architecture. The electrospinning parameters are identical to those employed in our earlier study of PAN/PVP/Nb_2O_5 nanofiber adsorbents to enable a direct comparison between the two filler systems.

Table 1. Sample designation and composition of the electrospinning dopes used in this study.

Sample	PAN (g)	PVP (g)	Zeolite (g)	DMF (mL)
PAN/PVP	0.8	0.5	0.0	10
PAN/PVP/Ze1	0.8	0.5	0.1	10
PAN/PVP/Ze3	0.8	0.5	0.3	10
PAN/PVP/Ze5	0.8	0.5	0.5	10

2.3 Materials characterization

Fiber morphology was examined using a scanning electron microscope (SEM, JEOL JSM-6510) operated at 15 kV, after sputter-coating the samples with a thin layer of Au. The elemental composition was obtained from energy-dispersive X-ray spectroscopy (EDS) integrated with the SEM. Mean fiber diameters and their standard deviations were determined from SEM micrographs by measuring at least 100 randomly selected individual fibers per sample using ImageJ software. Chemical bonding was investigated by Fourier-transform infrared spectroscopy (FTIR, Shimadzu IRSpirit) in attenuated-total-reflectance (ATR) mode over 4000–500 cm^{-1}. Crystallographic phase analysis was performed by X-ray diffraction (XRD, Rigaku SmartLab SE Basic) using Cu Kα radiation ($\lambda = 1.5406$ Å) over a 2θ range of 10–80°. UV-visible absorption spectra were recorded on a UV-Vis spectrophotometer over 400–800 nm.

2.4 Adsorption studies

The dye-removal performance of the nanofiber membranes was evaluated using methylene blue as a representative cationic dye. In each experiment, 0.05 g of membrane was immersed in 100 mL of a 10 ppm MB solution contained in a 100 mL glass beaker. A 5 mL aliquot was withdrawn immediately before adding the membrane to determine the initial concentration, C_0. The adsorption was conducted in the dark at room temperature with magnetic stirring at 400 rpm. Aliquots were withdrawn at predetermined intervals (10, 20, 30, 60, 120, 180, 240, and 300 min), and the residual MB concentration was determined from UV-Vis absorbance at 663 nm against a calibration curve built from 2, 5, 6, 8, and 10 ppm standards. The adsorption capacity at time t, q_t (mg g^{-1}), was calculated from the mass-balance expression

$$q_t = \frac{(C_0 - C_t)\,V}{m} \tag{1}$$

where C_0 and C_t (mg L^{-1}) are the initial and time-dependent dye concentrations, V (L) is the solution volume, and m (g) is the membrane mass.

The removal efficiency is given by

$$Removal\ (\%) = (C_0 - C_t)/C_0 \times 100 \tag{2}$$

2.5 Kinetic modelling

The kinetic behaviour of MB adsorption on the PAN/PVP/Zeolite nanofiber membranes was analysed using the linearized pseudo-first-order (PFO) and pseudo-second-order (PSO) models, expressed as

$$\log(q_e - q_t) = \log q_e - \frac{k_1}{2.303}\, t, \tag{3}$$

$$\frac{t}{q_t} = \frac{1}{k_2 q_e^2} + \frac{t}{q_e}, \tag{4}$$

where q_e and q_t are the adsorption capacities at equilibrium and at time t (mg g^{-1}), and k_1 (min^{-1}) and k_2 (g mg^{-1} min^{-1}) are the rate constants of the PFO and PSO models, respectively. Model adequacy was judged from the coefficient of determination (R^2) and the agreement between experimental q_t and model-fitted q_e; the model with higher R^2 and closer agreement with the experimental data was interpreted as the dominant kinetic regime.

3. Results and Discussion

3.1 Morphology and elemental composition

Figure 1 shows SEM micrographs of the four electrospun samples at three magnification levels (1000×, 3000×, and 10,000×), together with the fiber-diameter distributions obtained from ImageJ analysis of at least 100 fibers per sample. All four samples produced continuous, bead-free, randomly oriented nanofibers with a uniform three-dimensional network topology, indicating that the addition of natural zeolite up to 0.5 g does not destabilize the electrospinning jet. The mean fiber diameter increases monotonically with zeolite loading, from 626±57 nm for PAN/PVP to 725±68 nm for PAN/PVP/Ze1, 794±69 nm for PAN/PVP/Ze3, and 902±68 nm for PAN/PVP/Ze5. The narrow and comparable standard deviations (57–69 nm) across the four samples confirm that the diameter distributions remain similarly unimodal, while the steady shift of the mean reflects the increase in dope viscosity produced by the progressive incorporation of solid filler into the PAN/PVP/DMF solution. At 10,000× magnification, zeolite particles appear as nodular features that are embedded in or partially protrude from the polymer fibers rather than being deposited as loose aggregates on the surface, demonstrating that the spinning conditions successfully encapsulate the filler inside the fiber matrix [28].

The EDS spectra and quantitative elemental analysis of the four samples are shown in Figure 2, and the corresponding atomic-percent composition is summarized in the bar chart of Figure 3a. The pristine PAN/PVP membrane (Figure 2a) contains only C (22.99 wt%), N (44.70 wt%), and O (31.93 wt%), consistent with the nominal PAN/PVP chemistry, together with a negligible Al contribution (0.37 wt%) that can be attributed to EDS background. With the incorporation of natural zeolite, both Si and Al appear and increase monotonically across the loading series: Si rises from 4.38 wt% (Ze1, Figure 2b) to 9.54 wt% (Ze3, Figure 2c) and 10.68 wt% (Ze5, Figure 2d), while Al rises from 1.38 to 2.66 and 2.90 wt% over the same series. The same monotonic trend is clearly visible in atomic percent in Figure 3a. The Si/Al ratio remains in the range 3.2–3.7 across all three loadings, in good agreement with the stoichiometry expected for clinoptilolite and confirming that the crystalline framework of the aluminosilicate is transferred intact from the raw mineral to the nanofiber matrix [29,30]. Together, the SEM and EDS results demonstrate that the nanofiber architecture is preserved, the filler is genuinely embedded rather than merely deposited, and the effective zeolite content can be tuned proportionally to the mass of precursor added to the dope.

3.2 Structural and chemical characterization

The X-ray diffraction patterns of the four samples together with the natural-zeolite reference are presented in Figure 3b. All four membranes exhibit a broad halo centered at $2\theta \approx 17^\circ$, which is assigned to the (100) reflection of the semi-crystalline PAN backbone superimposed on the amorphous contribution of PVP. On top of this polymer halo, progressively sharper diffraction features attributable to clinoptilolite emerge as the zeolite content is increased. In PAN/PVP/Ze1, low-intensity reflections are already visible at $2\theta \approx 9.8^\circ$ and 11.2°, which are characteristic of the (020) and (200) planes of clinoptilolite [31,32,33]. In PAN/PVP/Ze3, a strong new reflection appears at $2\theta \approx 22.6^\circ$, and in PAN/PVP/Ze5 this peak sharpens further and is accompanied by an additional reflection at $2\theta \approx 29.6^\circ$, which is another diagnostic clinoptilolite feature. The progressive emergence and intensification of these reflections without the appearance of any secondary or shifted phase demonstrate that the crystalline aluminosilicate framework is preserved through electrospinning and the subsequent 200 °C heat treatment under N_2, and that the effective loading of clinoptilolite in the nanofiber matrix scales monotonically with the precursor mass.

The FTIR spectra in Figure 3c confirm the compositional integrity of the polymer matrix and the progressive incorporation of the zeolite filler. All samples show the characteristic bands of PAN/PVP: a broad O–H/N–H envelope near 3400 cm^{-1}, aliphatic C–H stretching around 2930 cm^{-1}, the sharp C≡N stretch of the PAN nitrile at ∼2242 cm^{-1}, the C=O stretch of the PVP pyrrolidone ring at ∼1659 cm^{-1}, CH_2 bending around 1450 cm^{-1}, and C–N/C–O backbone vibrations near 1288 cm^{-1}. These polymer-associated bands remain essentially unchanged in both position and relative intensity across all Ze-loaded samples, indicating that neither the compositing step nor the 200 °C thermal stabilization significantly disrupts the PAN/PVP chemistry. A new and growing absorption band associated with the asymmetric stretching vibration of Si–O–Si / Si–O–Al bonds emerges in the ∼1000–1100 cm^{-1} region [32,33]. Its position shifts progressively to lower wavenumber as the zeolite content increases, from 1067 cm^{-1} in PAN/PVP/Ze1 to 1042 cm^{-1} in PAN/PVP/Ze3 and 1040 cm^{-1} in PAN/PVP/Ze5, while the corresponding band depth deepens from ∼96% to ∼86% transmittance. A second, weaker Si–O band centered around 520–540 cm^{-1} follows the same trend. The red-shift and intensification of the aluminosilicate fingerprint, together with the unchanged polymer bands, provide clear spectroscopic evidence that clinoptilolite is successfully embedded in the PAN/PVP matrix and that its effective loading increases monotonically from Ze1 to Ze5, in full agreement with the XRD and EDS trends.

3.3 Methylene blue adsorption kinetics

The time-dependent UV-Vis absorption spectra of 10 ppm MB solutions exposed to each membrane, together with the derived adsorption kinetics, are shown in Figure 4. The characteristic MB absorption peak at 663 nm decreases monotonically with contact time for all four samples (Figure 4a–d), confirming progressive dye uptake. The rate and extent of the decrease, however, depend strongly on the zeolite content. For pristine PAN/PVP, the absorbance decreases only slowly

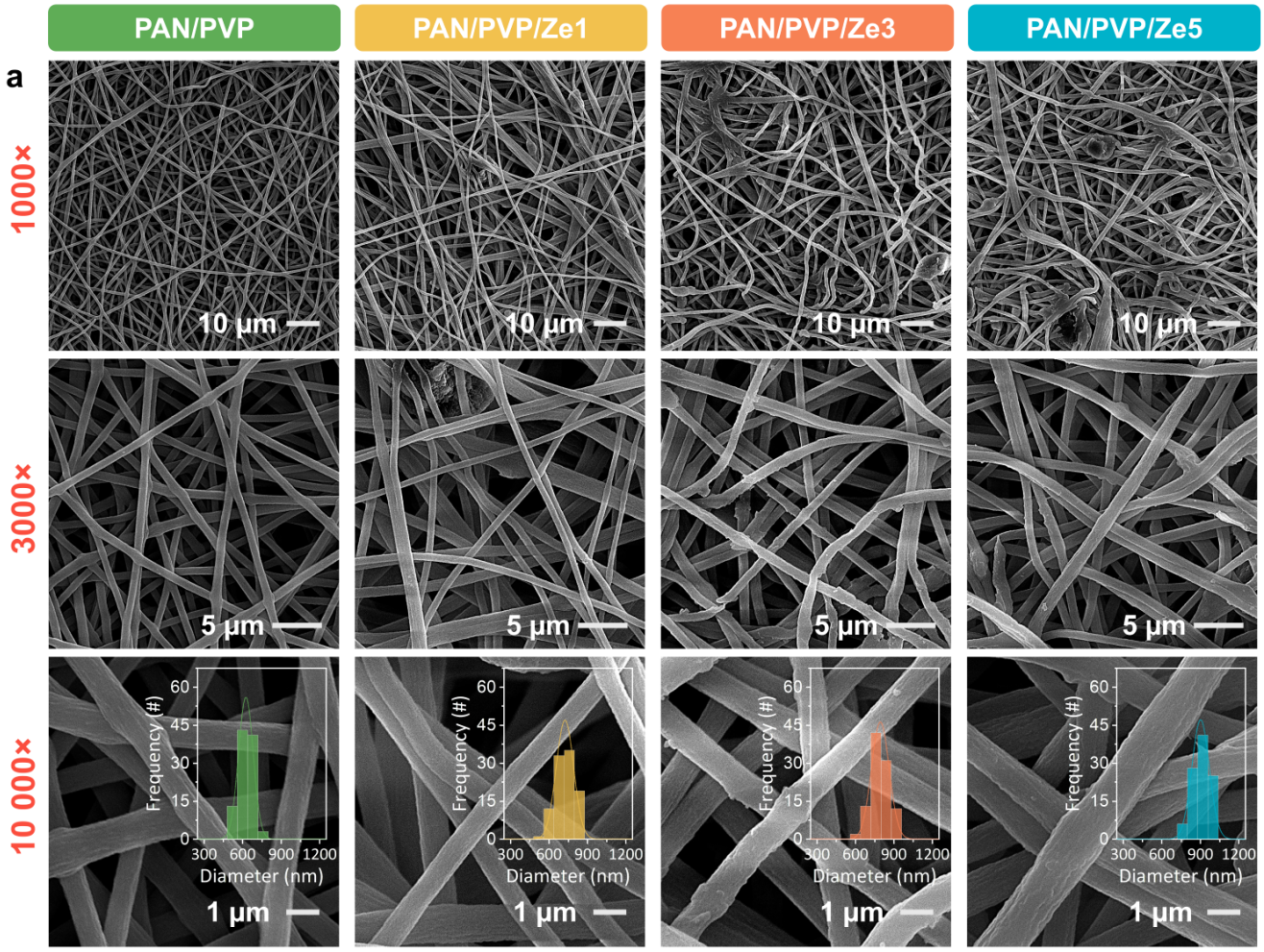

Figure 1. SEM images of electrospun (a) PAN/PVP, (b) PAN/PVP/Ze1, (c) PAN/PVP/Ze3, and (d) PAN/PVP/Ze5 nanofiber membranes after heat treatment at 200 °C, imaged at 1000×, 3000×, and 10,000× magnification. Bottom-row insets show the fiber-diameter distributions obtained from ImageJ analysis ($n \geq 100$ per sample).

and retains a clearly visible peak at 300 min, corresponding to ∼58.7% removal and an experimental adsorption capacity of 8.2 mg g^{-1}. The introduction of even a modest amount of zeolite dramatically accelerates the uptake: PAN/PVP/Ze1 reaches 91.7% removal (12.8 mg g^{-1}), PAN/PVP/Ze3 reaches 96.5% removal (13.5 mg g^{-1}), and PAN/PVP/Ze5 reaches essentially complete removal (∼100%, 14.0 mg g^{-1}) within the same 300 min. The time-resolved adsorption-capacity curves in Figure 4e confirm this monotonic enhancement and show a classical two-stage profile for all samples: a fast initial uptake within the first 30–60 min, during which the majority of the accessible surface sites are rapidly populated, followed by a gradual approach to equilibrium as the remaining sites are filled.

The linearized PFO and PSO plots are shown in Figure 4f and Figure 4g, and the corresponding fitted parameters are collected in Table 2. The PSO model describes the data consistently better than the PFO model across the entire loading series: the PSO coefficient of determination is uniformly high ($R^2 \geq 0.984$ for all samples, with $R^2 = 0.996$ for PAN/PVP, PAN/PVP/Ze1, and 0.993 for PAN/PVP/Ze3), whereas the PFO fit degrades noticeably at low loading, reaching $R^2 = 0.885$ for the pristine PAN/PVP control. Furthermore, the PSO-fitted q_e values are in close agreement with the experimentally observed adsorption capacities at 300 min, while the PFO-fitted values systematically underestimate them by roughly a factor of two. This combined evidence, namely the higher R^2 and closer agreement with the experimental plateau, identifies the PSO model as the dominant kinetic regime and suggests that MB adsorption on the PAN/PVP/Zeolite nanofiber membranes is rate-limited by a chemisorption-type surface interaction rather than by pure film diffusion. The PFO rate constant k_1 increases from 0.010 to 0.021 min^{-1} as the zeolite content increases from 0 to 0.5 g, reflecting the faster uptake observed in Figure 4e. The PSO rate constant k_2 decreases from 0.007 to 0.001 g mg^{-1} min^{-1} over the same series; this decrease does not indicate a slowdown of the real kinetics but arises from the inverse q_e^2 dependence of the PSO expression, which mathematically couples a rising q_e to a declining k_2. We note that the PSO-fitted q_e values for PAN/PVP/Ze3 and PAN/PVP/Ze5 (16.08 and 16.69 mg g^{-1}, respectively) exceed the instantaneous mass-balance ceiling $C_0V/m \approx 13.96$ mg g^{-1} at the measured initial concentration; this is a known characteristic of the linearized PSO model, whose fitted q_e is an asymptotic extrapolation of the t/q_t vs t regression rather than a direct

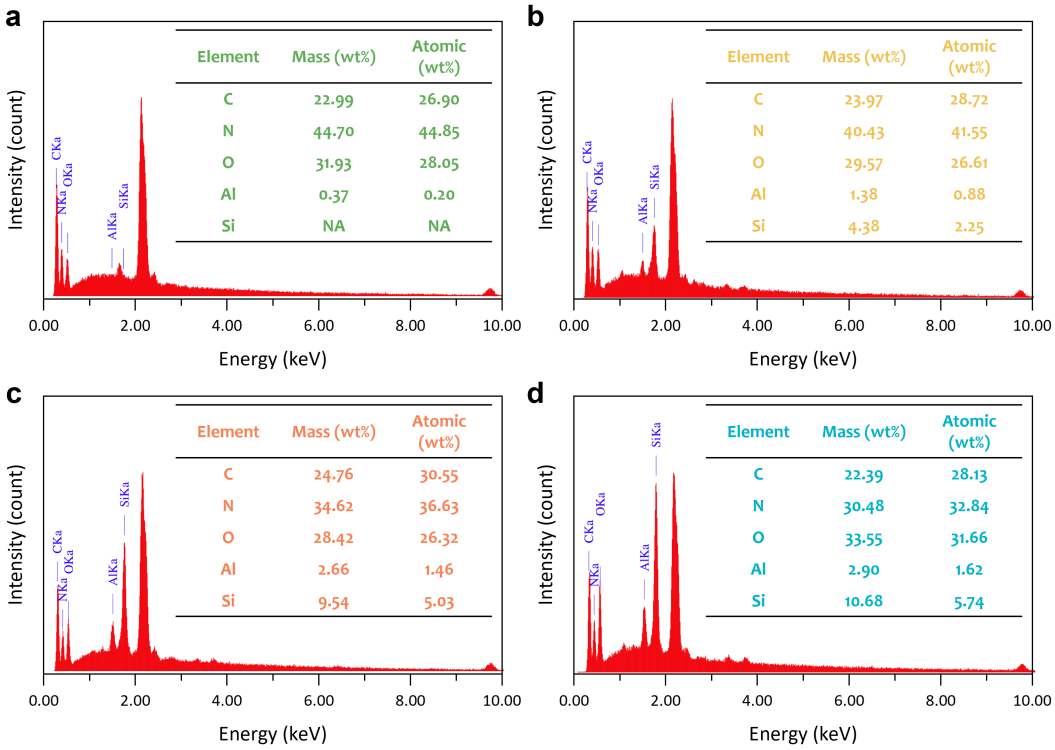

Figure 2. EDS spectra and quantitative elemental composition (wt% and atomic %) of (a) PAN/PVP, (b) PAN/PVP/Ze1, (c) PAN/PVP/Ze3, and (d) PAN/PVP/Ze5 nanofiber membranes.

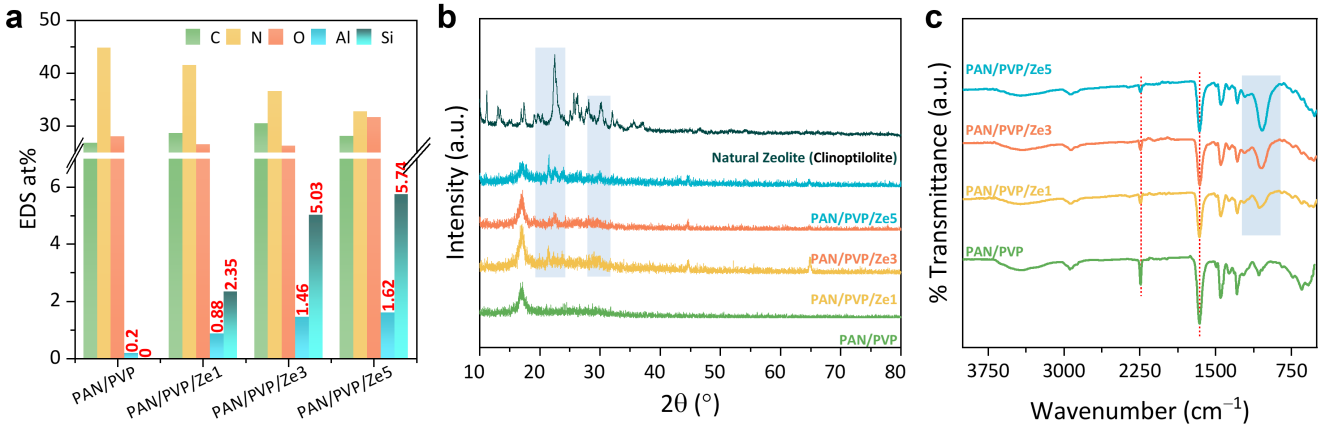

Figure 3. (a) Quantitative EDS elemental composition (at%) of C, N, O, Al, and Si for all four nanofiber membranes. (b) X-ray diffraction patterns of natural zeolite (clinoptilolite), PAN/PVP, PAN/PVP/Ze1, PAN/PVP/Ze3, and PAN/PVP/Ze5 nanofiber membranes; shaded bands highlight the main clinoptilolite reflections at $2\theta \approx 22^{\circ}$ and 30°. (c) Fourier-transform infrared spectra of the same samples; the shaded region highlights the Si–O–Si / Si–O–Al asymmetric stretching band.

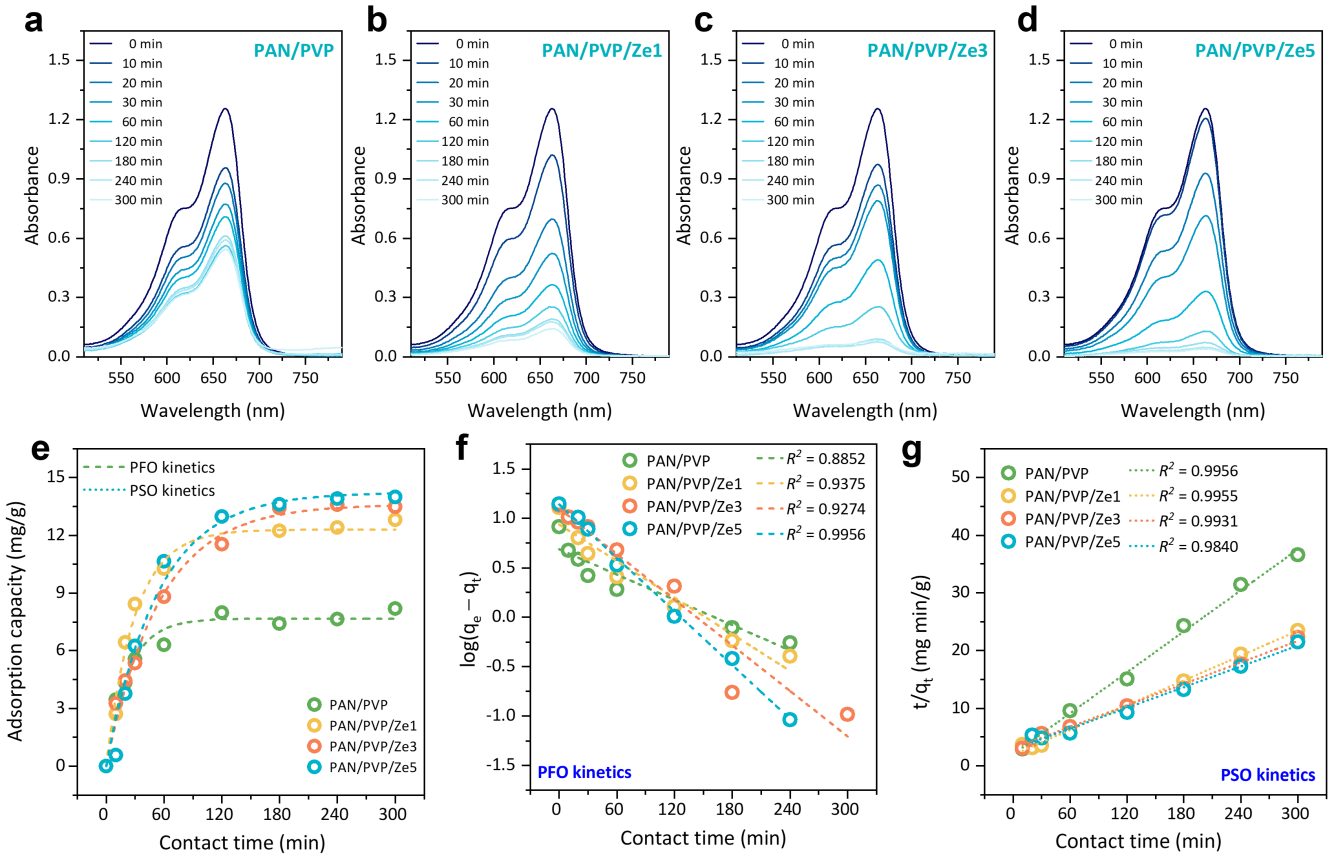

Figure 4. Methylene blue (10 ppm) adsorption by (a) PAN/PVP, (b) PAN/PVP/Ze1, (c) PAN/PVP/Ze3, and (d) PAN/PVP/Ze5 nanofiber membranes monitored by UV-Vis spectroscopy over 0–300 min. (e) Adsorption capacity q_t as a function of contact time with pseudo-first-order (PFO, dashed) and pseudo-second-order (PSO, solid) kinetic fits. (f) PFO linearization $\log(q_e - q_t)$ vs t. (g) PSO linearization t/q_t vs t. Adsorption conditions: 0.05 g membrane, 100 mL of 10 ppm MB solution, 400 rpm stirring in the dark, room temperature.

experimental quantity, and should be interpreted as the equilibrium capacity predicted by the model if the experiment were run to infinite time.

The mechanistic picture that emerges from the combined SEM/EDS/XRD/FTIR/kinetic results is internally consistent. Pristine PAN/PVP already exhibits moderate MB uptake thanks to the polar nitrile groups on the PAN backbone, which can engage in dipolar and π–π interactions with the aromatic framework of the cationic dye. Adding natural zeolite introduces a much larger density of high-affinity sites for MB^+: the negatively charged aluminosilicate framework provides electrostatic attraction for cations, the exchangeable Na^+, K^+, and Ca^{2+} cations in the clinoptilolite channels enable direct cation-exchange uptake, and the internal microporosity further contributes through physical pore filling. Because the effective zeolite content in the fiber rises monotonically with the precursor mass (as shown by the Si/Al EDS values in Figures 2 and 3a, the intensifying clinoptilolite XRD reflections in Figure 3b, and the deepening Si–O–Si/Si–O–Al FTIR band in Figure 3c), the density of these high-affinity sites increases in the same order, explaining the PAN/PVP < Ze1 < Ze3 < Ze5 ranking of both the initial uptake rate and the equilibrium adsorption capacity. PAN/PVP/Ze5 removes essentially all MB from solution within 300 min at 10 ppm, demonstrating the practical effectiveness of the composite under conditions representative of dilute textile effluents.

4. Conclusions

Electrospun PAN/PVP nanofiber membranes loaded with 0.1, 0.3, and 0.5 g of natural zeolite (clinoptilolite) from Tanggamus, Indonesia, were successfully prepared and thermally stabilized at 200 °C under N_2, and their morphology, composition, structure, chemistry, and MB adsorption kinetics were characterized in detail. SEM imaging revealed continuous, bead-free fibers whose mean diameter increased monotonically from 626 to 902 nm with zeolite loading, and EDS confirmed a parallel rise in Si (up to 10.68 wt%) and Al (up to 2.90 wt%) with a Si/Al ratio consistent with clinoptilolite. XRD showed the progressive emergence of clinoptilolite reflections at $2\theta \approx 9.8^\circ$, 22.5°, and 29.6°, and FTIR showed a red-shifting and intensifying Si–O–Si/Si–O–Al asymmetric stretching band (1067 $\rightarrow$ 1040 cm^{-1}) alongside unchanged PAN (C≡N at 2242 cm^{-1}) and PVP (C=O at 1659 cm^{-1}) signatures, jointly demonstrating that the aluminosilicate framework is preserved and its effective loading scales with the precursor mass without disturbing the polymer host. In 10 ppm MB adsorption tests, zeolite loading systematically enhanced both the uptake rate and the equilibrium capacity, culminating in essentially complete (~100%) dye removal by PAN/PVP/Ze5 at 300 min with an experimental capacity of 14.0 mg g^{-1}, compared with 58.7% and 8.2 mg g^{-1} for the pristine PAN/PVP control. The kinetic data were well de-

Table 2. Pseudo-first-order (PFO) and pseudo-second-order (PSO) kinetic parameters for methylene blue (MB) adsorption (10 ppm, 100 mL, 0.05 g adsorbent) onto PAN/PVP and PAN/PVP/Zeolite nanofiber membranes.

Adsorbent	PFO kinetics			PSO kinetics		
	q_e (mg g^{-1})	k_1 (min^{-1})	R^2	q_e (mg g^{-1})	k_2 (g mg^{-1} min^{-1})	R^2
PAN/PVP	4.86	0.010	0.8853	8.44	0.007	0.9956
PAN/PVP/Ze1	8.68	0.014	0.9376	13.96	0.003	0.9955
PAN/PVP/Ze3	12.57	0.018	0.9274	16.08	0.001	0.9931
PAN/PVP/Ze5	13.86	0.021	0.9956	16.69	0.001	0.984

scribed by the pseudo-second-order model ($R^2 \geq 0.984$ for all samples), identifying a chemisorption-controlled mechanism governed by electrostatic attraction, cation exchange, and micropore filling at the clinoptilolite sites. These results establish natural-zeolite-loaded PAN/PVP nanofiber membranes as an effective, low-cost, and recoverable platform for cationic-dye wastewater treatment. Future work will address reusability over multiple adsorption/regeneration cycles, equilibrium isotherm and thermodynamic analyses, the selectivity of the composite toward anionic dyes, and tests on real textile effluents.

DATA AVAILABILITY STATEMENT

The datasets generated and analysed during this study are available from the corresponding author upon reasonable request.

CONFLICT OF INTEREST

The authors declare no conflict of interest.

FUNDING

This study received no specific funding.

AUTHOR CONTRIBUTIONS

SFA: Investigation, Formal analysis, Writing – Original Draft. **IRH:** Conceptualization, Supervision, Writing – Review & Editing. **RA:** Resources, Formal analysis. **AR:** Methodology, Conceptualization, Supervision, Writing – Review & Editing, Funding acquisition. All authors approved the final manuscript.

REFERENCES

[1] Fried R, Oprea I, Fleck K, Rudroff F. Biogenic colourants in the textile industry – a promising and sustainable alternative to synthetic dyes. *Green Chemistry*. 2022;24(1):13-35. doi:10.1039/d1gc02968a.

[2] Islam T, Repon MR, Islam T, Sarwar Z, Rahman MM. Impact of textile dyes on health and ecosystem: a review of structure, causes, and potential solutions. *Environmental Science and Pollution Research*. 2022;30(4):9207-9242. doi:10.1007/s11356-022-24398-3.

[3] Yang Y, Zhu Q, Peng X, Sun J, Li C, Zhang X, Zhang H, Chen J, Zhou X, Zeng H, Zhang Y. Hydrogels for the removal of the methylene blue dye from wastewater: a review. *Environmental Chemistry Letters*. 2022;20(4):2665-2685. doi:10.1007/s10311-022-01414-z.

[4] Mussa ZH, Al-Ameer LR, Al-Qaim FF, Deyab IF, Kamyab H, Chelliapan S. A comprehensive review on adsorption of methylene blue dye using leaf waste as a bio-sorbent: isotherm adsorption, kinetics, and thermodynamics studies. *Environmental Monitoring and Assessment*. 2023;195(8). doi:10.1007/s10661-023-11432-1.

[5] Chahal M, Kumari S, Bhattacharya A, Garg MC. Evaluating sustainable agricultural waste biomass for methylene blue adsorption in wastewater treatment: A state-of-the-art review. *Bioresource Technology Reports*. 2024;28:101983. doi:10.1016/j.biteb.2024.101983.

[6] Sangamnere R, Misra T, Bherwani H, Kapley A, Kumar R. A critical review of conventional and emerging wastewater treatment technologies. *Sustainable Water Resources Management*. 2023;9(2). doi:10.1007/s40899-023-00829-y.

[7] Zhao Y, Chang C, Ji H, Li Z. Challenges of petroleum wastewater treatment and development trends of advanced treatment technologies: A review. *Journal of Environmental Chemical Engineering*. 2024;12(5):113767. doi:10.1016/j.jece.2024.113767.

[8] Bera SP, Godhaniya M, Kothari C. Emerging and advanced membrane technology for wastewater treatment: A review. *Journal of Basic Microbiology*. 2021;62(3-4):245-259. doi:10.1002/jobm.202100259.

[9] Li J, Cao Y, Ding K, Ye J, Li F, Ma C, Lv P, Xu Y, Shi L. Research progress of industrial wastewater treatment technology based on solar interfacial adsorption coupled evaporation process. *Science of The Total Environment*. 2024;931:172887. doi:10.1016/j.scitotenv.2024.172887.

[10] Oladoye PO, Kadhom M, Khan I, Hama Aziz KH, Alli YA. Advancements in adsorption and photodegradation technologies for Rhodamine B dye wastewater treatment: fundamentals, applications, and future directions. *Green Chemical Engineering*. 2024;5(4):440-460. doi:10.1016/j.gce.2023.12.004.

[11] Gado MG, Nasser M, Hassan AA, Hassan H. Adsorption-based atmospheric water harvesting powered by solar energy: Comprehensive review on desiccant materials and systems. *Process Safety and Environmental Protection*. 2022;160:166-183. doi:10.1016/j.psep.2022.01.061.

[12] Kurisingal JF, Yun H, Hong CS. Porous organic materials for iodine adsorption. *Journal of Hazardous Materials*. 2023;458:131835. doi:10.1016/j.jhazmat.2023.131835.

[13] Alsaman AS, Maher H, Ghazy M, Ali ES, Askalany AA, Baran Saha B. 2D materials for adsorption desalination applications: A state of the art. *Thermal Science and Engineering Progress*. 2024;49:102455. doi:10.1016/j.tsep.2024.102455.

[14] Bahrudin NN, Nawi MA, Sabar S. Immobilized chitosan-montmorillonite composite adsorbent and its photocatalytic regeneration for the removal of methyl orange. *Reaction Kinetics, Mechanisms and Catalysis*. 2019;126(2):1135-1153. doi:10.1007/s11144-019-01536-6.

[15] Awual MR, Hasan MM, Shahat A, Naushad M, Shiwaku H, Yaita T. Investigation of ligand immobilized nano-composite adsorbent for efficient cerium(III) detection and recovery. *Chemical Engineering Journal*. 2015;265:210-218. doi:10.1016/j.cej.2014.12.052.

[16] Kang SB, Wang Z, Zhang W, Kim KY, Won SW. Removal of short- and long-chain PFAS from aquatic systems using electrostatic attraction of polyethylenimine-polyvinyl chloride electrospun nanofiber adsorbent. *Separation and Purification Technology*. 2023;326:124853. doi:10.1016/j.seppur.2023.124853.

[17] Xu X, Lv H, Zhang M, Wang M, Zhou Y, Liu Y, Yu DG. Recent progress in electrospun nanofibers and their applications in heavy metal wastewater treatment. *Frontiers of Chemical Science and Engineering*. 2023;17(3):249-275. doi:10.1007/s11705-022-

2245-0.

[18] Rianjanu A, Fauzi F, Triyana K, Wasisto HS. Electrospun Nanofibers for Quartz Crystal Microbalance Gas Sensors: A Review. *ACS Applied Nano Materials*. 2021;4(10):9957-9975. doi:10.1021/acsanm.1c01895.

[19] Aflaha R, Putri LA, Farrel A, Anzinger S, Rianjanu A, Yulianto N, Fueldner M, Roto R, Peiner E, Wasisto HS, Triyana K. Crafting high-temperature stable and hydrophobic nanofiber membranes for particulate matter filtration. *Communications Materials*. 2025;6(1). doi:10.1038/s43246-025-00799-y.

[20] Wang Z, Li J, Li S, Li D, Zhao Y, Xu L, Liu G, Chen Z, Luo X. Tannic acid-etched PAN/PVP nanofibers loaded with Cu-MOFs enhance antibacterial efficacy and accelerate wound healing. *Colloids and Surfaces B: Biointerfaces*. 2025;253:114719. doi:10.1016/j.colsurfb.2025.114719.

[21] Kang Y, Chen J, Feng S, Zhou H, Zhou F, Low ZX, Zhong Z, Xing W. Efficient removal of high-temperature particulate matters via a heat resistant and flame retardant thermally-oxidized PAN/PVP/SnO2 nanofiber membrane. *Journal of Membrane Science*. 2022;662:120985. doi:10.1016/j.memsci.2022.120985.

[22] Yuan Z, Zhang J, Zhao X, Liu S, Yu S, Liu X, Zhang X, Yi X. A multifunctional PAN/PVP nanofiber sponge wound dressing loaded with ZIF-8-derived carbon nanoparticles with adjustable wetness for rapid wound disinfection and exudate management. *Journal of Materials Chemistry B*. 2023;11(34):8216-8227. doi:10.1039/d3tb01119d.

[23] Biblioteca I, Sambucci M, Valente M. Zeolite-Clinoptilolite conditioning for improved heavy metals ions removal: A preliminary assessment. *Ceramics International*. 2023;49(23):39649-39656. doi:10.1016/j.ceramint.2023.09.319.

[24] Grifasi N, Ziantoni B, Fino D, Piumetti M. Fundamental properties and sustainable applications of the natural zeolite clinoptilolite. *Environmental Science and Pollution Research*. 2024;32(48):27805-27840. doi:10.1007/s11356-024-33656-5.

[25] Mutalib NFAA, Seitkhan A, Othman MBH, Ramle AQ, Salleh NM, Othman MHD, Hubadillah SK, Jamalludin MR, Yusof NN, Adam MR. Revolutionizing dye removal in wastewater: An optimization study of curcumin-functionalized zeolite beads for methylene blue adsorption. *Surfaces and Interfaces*. 2025;72:107434. doi:10.1016/j.surfin.2025.107434.

[26] He W, Zhang M, Du H, Amrane A, Yu H, Liu Y. Anchoring nano-zeolite NaX particles on polydopamine-modified PVDF/PAN electrospun membranes for enhancing interception, adsorption and antifouling performance. *Colloids and Surfaces A: Physicochemical and Engineering Aspects*. 2023;670:131587. doi:10.1016/j.colsurfa.2023.131587.

[27] Arif MF, Muhtar SA, Siburian C, Marpaung KDP, Yulianto N, Abdi FF, Taher T, Wasisto HS, Rianjanu A. Zeolite-PAN/PVDF composite nanofiber membranes for highly efficient and selective removal of cationic dyes from wastewater. *Case Studies in Chemical and Environmental Engineering*. 2024;10:100806. doi:10.1016/j.cscee.2024.100806.

[28] Cai Z, Park J, Park S. Synergistic effect of Pd and Fe2O3 nanoparticles embedded in porous NiO nanofibers on hydrogen gas detection: Fabrication, characterization, and sensing mechanism exploration. *Sensors and Actuators B: Chemical*. 2023;388:133836. doi:10.1016/j.snb.2023.133836.

[29] Kadium AH, Sharif JA, Akhgar BN. Evaluating microstructure and surface changes of clinoptilolite after mechanical activation. *Colloids and Surfaces A: Physicochemical and Engineering Aspects*. 2025;713:136523. doi:10.1016/j.colsurfa.2025.136523.

[30] Mohammadzadeh Kakhki R, Zirjanizadeh S, Mohammadpoor M. A review of clinoptilolite, its photocatalytic, chemical activity, structure and properties: in time of artificial intelligence. *Journal of Materials Science*. 2023;58(26):10555-10575. doi:10.1007/s10853-023-08643-9.

[31] Ikhsan F, Muhtar SA, Aflaha R, Adhika DR, Muhyi A, Triyana K, Khairurrijal K, Taher T, Rianjanu A, Arif MF. Glycerol-Assisted Modification of 3D-Printed Zeolite (3D-Ze/Gy) for Enhanced Methylene Blue Dye Removal in Aqueous Solutions. *Advanced Engineering Materials*. 2025;27(9). doi:10.1002/adem.202402555.

[32] Taher T, Muhtar SA, Sianturi AGN, Aflaha R, Triyana K, Lesbani A, Arif MF, Hapidin DA, Khairurrijal K, Yu Z, Rianjanu A. 3D-printed Zeolite–MgAl layered double oxides (3D-Ze/LDO) as a reusable adsorbent with dual functionality for effective anionic and cationic pollutant removal from water. *Applied Clay Science*. 2025;278:108009. doi:10.1016/j.clay.2025.108009.

[33] Fitri A, Prasetya B, Aini Q, Ikhsan F, Aflaha R, Triyana K, Taher T, Arif MF, Rianjanu A. Enhanced methylene blue adsorption capacity of 3D-printed zeolite/glycerol (3D-Ze/Gy) by sintering temperature optimalizations. *Next Materials*. 2025;9:101069. doi:10.1016/j.nxmate.2025.101069.

